PHYSICAL REVIEW D **81,** 044003 (2010)

Stability, causality, and quasinormal modes of cosmic strings and cylinders

Alan B. Pavan* and E. Abdalla†

Instituto de Física, Universidade de São Paulo, Caixa Postal 66318, 05315-970, São Paulo-SP, Brazil

C. Molina‡

Escola de Artes, Ciências e Humanidades, Universidade de São Paulo, Avenida Arlindo Bettio 1000, CEP 03828-000, São Paulo-SP, Brazil

(Received 28 August 2009; published 1 February 2010)

In this work we consider the evolution of a massive scalar field in cylindrically symmetric space-times. Quasinormal modes have been calculated for static and rotating cosmic cylinders. We found unstable modes in some cases. Rotating as well as static cosmic strings, i.e., without regular interior solutions, do not display quasinormal oscillation modes. We conclude that rotating cosmic cylinder space-times that present closed timelike curves are unstable against scalar perturbations.

DOI: 10.1103/PhysRevD.81.044003 PACS numbers: 04.30.Nk, 04.20.Ex

I. INTRODUCTION

Cylindrically symmetric space-times, cosmic strings, and cosmic cylinders, in particular, are an important subclass of the full axial geometries, with a symmetry structure in many ways more complex than the spherically symmetric backgrounds. Although not compatible with asymptotic flatness, cylindrical solutions have been studied in many different physically meaningful contexts. Definitions and structural aspects have been investigated in [1,2]. In cosmology and astrophysics they have been used to model the formation of structure [3], gravitational lensing effect [4], and gamma ray bursts [5]. In condensed matter, they appear in the study of superconductivity and topological defects [6].

Besides formalism issues and phenomenological applications, cosmic strings display a variety of different phenomena. They are important for the study of Einstein general relativity in extreme situations, where the limits of the theory can be explored and information about very new phenomena can be gathered. For example, they have been used to model time machines[7–9]. Cylindrical space-times frequently have cuts in the angular variable. Where there is a rotation, one can imagine a voyager along the angular direction with an effectively superluminal velocity in a closed space-time path, hence a time machine. Thus, such geometries are generally associated with the possibility of traveling back in time, always a puzzling possibility [10–12]. Hence the question whether these space-times are physically feasible. Effective superluminal velocities are not necessarily a pathology. For instance, in [13], it has been shown that in braneworlds a gravitational sign can be sent through the bulk in a way that it can reach a distant point in the brane faster than light propagating in the brane. However, such signs seem to be irrelevant, because most of them advance, compared to a light sign, by negligibly small amounts.

If we take causality as a fundamental principle, it is reasonable to conjecture that time machines cannot be constructed in the real world, although they are possible as exact solutions of Einstein equations. It is expected that these time machines do not survive as physical solutions, but we do not yet know any physical mechanism that prohibits the existence of such backgrounds.

In this work, we propose such mechanism, associating closed timelike curves to instabilities in certain cylindrical geometries. Taking the spherically symmetric cases as reference, not much has been stated about the stability of cosmic strings. This is specially true for rotating cosmic strings, which are relevant for time machine theoretical proposals. One exception, in the braneworld context, is the well known Gregory-Laflamme [14] instability in the black strings.

We have calculated the evolution of a massive scalar field propagating in different cosmic string and cosmic cylinder backgrounds. The relevant boundary conditions to be satisfied by a massive scalar field are presented. These conditions will be part of the quasinormal mode definition, which will be calculated considering these backgrounds. The static cases will be treated in the first place, because the rotating geometries present closed timelike curves (CTCs) and in these cases additional analysis is necessary to render the problem tractable. Analyzing the behavior of the field and their quasinormal modes we could present evidence of the stability of some of these space-times.

II. COSMIC STRING AND CYLINDER SPACE-TIMES

The metric of a stationary and cylindrically symmetric space-time is given by an expression of the form

$$ds^2 = -\tilde{F}dt^2 + 2\tilde{M}dtd\phi + \tilde{L}d\phi^2 + \tilde{H}dr^2 + \tilde{S}dz^2, \quad (1)$$

*alan@fma.if.usp.br
†eabdalla@usp.br
‡cmolina@usp.br

where $(\tilde{F}, \tilde{M}, \tilde{L}, \tilde{H}, \tilde{S})$ are functions only of the radial coordinate r. All space-times studied here are described by this ansatz.

We start with the static cosmic cylinder background. It was obtained by Gott and Hiscock [4,15] and its exterior solution is given by

$$ds^2 = -dt^2 + dr^2 + dz^2 + (1-4\mu)^2 r^2 d\phi^2, \quad (2)$$

where the coordinates ranges are $-\infty < t < \infty$, $\bar{r}_0 \sin(\theta_M)(1-4\mu)^{-1} < r < \infty$, $0 \le \phi < 2\pi$, and $-\infty < z < \infty$. The interior solution is given by

$$ds^2 = -dt^2 + dr^2 + dz^2 + \bar{r}_0^2 \sin(r/\bar{r}_0)^2 d\phi^2, \quad (3)$$

with $-\infty < t < \infty$, $0 \le r \le \bar{r}_0\theta_M$, $0 \le \phi < 2\pi$, $-\infty < z < \infty$ and μ is the linear mass density. The matching point is defined by $r = r_b$ in the exterior radial coordinate and the corresponding interior radial coordinate is $r = r_s$. They are related by

$$r_b = \frac{\bar{r}_0 \sin(\theta_M)}{1-4\mu}, \qquad r_s = \bar{r}_0 \theta_M. \quad (4)$$

The other constants are related as

$$\mu = \frac{1}{4}[1 - \cos(\theta_M)], \qquad \rho = \frac{1}{8\pi \bar{r}_0^2}, \quad (5)$$

where ρ is the energy density. The static cosmic string space-time can be obtained taking the limit $\bar{r}_0 \to 0$. For both static cosmic string and cosmic cylinder, we have assumed $\mu < 1/4$. Additional details are presented in [4]. The restriction on μ leads to

$$\theta_M = \frac{r_s}{\bar{r}_0} < \frac{\pi}{2}. \quad (6)$$

The rotating cosmic cylinder solution was obtained by Jensen and Soleng [9]. The exterior solution reads

$$ds^2 = -dt^2 + dr^2 + dz^2 - 8J d\phi dt + [(1-4\mu)^2 (r + r_0)^2 - 16J^2] d\phi^2, \quad (7)$$

where μ is the linear mass density and J the rate of angular momentum per unit length. The constant r_0 determines the origin of the exterior radial coordinate. For

$$r + r_0 < \frac{4|J|}{1-4\mu} \quad (8)$$

this space-time exhibits closed timelike curves.

Inside the cylinder there are at least two possible regular solutions. The first scenario considered in this work is the ''flower pot'' model,

$$ds^2 = -\left[1 + \frac{16J^2}{r_s^4}(r_s^2 - r^2)\right] dt^2 - \frac{8Jr^2}{r_s^2} d\phi dt + r^2 d\phi^2 + dr^2 + dz^2, \quad (9)$$

where r_s is related to the exterior parameter r_0 by

$$r_0 = \pm \sqrt{\frac{r_s^2 + 16J^2}{(1-4\mu)^2}} - r_s. \quad (10)$$

Here there is no closed timelike curve.

The second type of internal solution treated is the so-called ''ballpoint pen'' model. It describes gravity generated by the following distribution of matter,

$$8\pi\rho = \lambda + \Omega^2, \qquad \Omega = \alpha\lambda(r_s - r), \quad (11)$$

where $\alpha \le 1$ is an arbitrary constant which can be adjusted such that we may or may not have closed timelike curves. This interior solution is described by

$$ds^2 = -dt^2 - 2M d\phi dt + \frac{\sin(\sqrt{\lambda} r)^2}{\lambda} - M^2 d\phi^2 + dr^2 + dz^2, \quad (12)$$

$$M = 2\alpha\left[(r - r_s)\cos(\sqrt{\lambda} r) - \frac{\sin(\sqrt{\lambda} r)}{\sqrt{\lambda}} + r_s\right]. \quad (13)$$

Imposing that exterior and interior solutions match continuously on the boundary r_s of the rotating cosmic cylinder, the parameters are related by

$$r_0 = \left[\pm \frac{\sqrt{1 - (1-4\mu)^2}}{(1-4\mu)\arccos(1-4\mu)} - 1\right] r_s, \qquad \sqrt{\lambda} = \frac{\arccos(1-4\mu)}{r_s}, \quad (14)$$

$$\mu = \frac{1 - \cos(\sqrt{\lambda} r_s)}{4}, \qquad J = \frac{2\alpha}{4}\left[r_s - \frac{\sin(\sqrt{\lambda} r_s)}{\sqrt{\lambda}}\right]. \quad (15)$$

III. EVOLUTION OF A MASSIVE SCALAR FIELD

The evolution of a minimally coupled massive scalar field Ψ in a curved space-time is given by the equation

$$\Box \Psi(t, r, \theta, z) = \beta^2 \Psi(t, r, \theta, z), \quad (16)$$

where β is the mass of the field and the differential operator $\Box$ has the form

$$\Box \Psi = \frac{1}{\sqrt{-g}} \partial_\mu (\sqrt{-g} g^{\mu\nu} \partial_\nu \Psi) \quad (17)$$

and g is the determinant of the metric. In the cylindrically symmetric space-time given by metric (1) we have

$$-\tilde{L}\partial_t^2 \Psi + \tilde{F}\partial_\phi^2 \Psi + 2\tilde{M}\partial_t(\partial_\phi \Psi) + \frac{1}{2}\frac{\partial_r(\chi \tilde{H}\tilde{S})}{\tilde{H}^2 \tilde{S}} \partial_r \Psi + \chi \partial_r\left(\frac{\partial_r \Psi}{\tilde{H}}\right) + \chi \partial_z\left(\frac{\partial_z \Psi}{\tilde{S}}\right) = \chi \beta^2 \Psi, \quad (18)$$

where $\mathcal{X} = \tilde{F}\tilde{L} + \tilde{M}^2$.

Since the space-time is stationary and invariant by translation in z and rotations in ϕ, the scalar field can be decomposed as

$$\Psi(t, r, \phi, z) = \sum_{m\in\mathbb{Z}} \int_{-\infty}^{\infty} \tilde{R}_{km}(t, r) e^{i(m\phi + kz)} dk, \tag{19}$$

where m is an integer number and k is real. We will be interested in a quasinormal mode decomposition, and therefore we also consider a "time-independent" approach, based on a Laplace-like transform [16]

$$R(\omega, r) = \int_0^{\infty} \tilde{R}_{km}(t, r) e^{i\omega t} dt, \tag{20}$$

with ω extended to the complex plane. Substituting (19) and (20) in (18), we observe that this latter differential equation is separable and can be written as

$$\frac{1}{2}\frac{\partial_r(\mathcal{X}\tilde{H}\tilde{S})}{\tilde{H}^2\tilde{S}}\partial_r R + \mathcal{X}\partial_r\left(\frac{\partial_r R}{\tilde{H}}\right) = R[\mathcal{X}(\beta^2 + k^2) + \tilde{F}m^2 - 2\tilde{M}m\omega - \tilde{L}\omega^2]. \tag{21}$$

The evolution of Ψ in the exterior region of the cosmic cylinders, describing the vacuum, can be calculated straightforwardly. The radial evolution of the massive scalar field in the exterior of a rotating cosmic cylinder is given by

$$x^2\frac{d^2R}{dx^2} + x\frac{dR}{dx} + R\left[(\omega^2 - k^2 - \beta^2)x^2 - \frac{(m + 4J\omega)^2}{(1 - 4\mu)^2}\right] = 0, \tag{22}$$

where we defined the coordinate $x = (r + r_0)$. Particular cases can be recovered: the static cosmic string and outside of the static cosmic cylinder setting ($J = r_0 = 0$) and the rotating cosmic string setting $r_0 = 0$. If $\omega^2 > k^2 + \beta^2$ Eq. (22) has an exact solution given in terms of Bessel functions. When $\omega^2 < k^2 + \beta^2$ Eq. (22) has an exact solution given in terms of the modified Bessel functions decaying exponentially to zero at spatial infinity. Therefore, we will analyze only the condition $\omega^2 > k^2 + \beta^2$ since, to calculate the quasinormal modes, we want that the field behaves as an outgoing traveling wave at spatial infinity.

For the interior of the static cosmic cylinder, the radial evolution of the scalar field has been obtained exactly. Applying (21) to the respective metric given by (3) we have

$$\frac{d^2R}{dx^2} + \frac{1}{\tan(x)}\frac{dR}{dx} + R\left[(\omega^2 - k^2 - \beta^2)\bar{r}_0^2 - \frac{m^2}{\sin^2(x)}\right] = 0, \tag{23}$$

where the radial coordinate $x = \bar{r}_0/r$ has been used. Equation (23) has an exact solution in terms of the associated Legendre functions.

For the flower pot model the function $\mathcal{X}$ and the radial derivative of the determinant of the metric g are

$$\mathcal{X} = r^2\sigma_1^2 = -g, \qquad \sigma_1^2 = \left(\frac{r_s^2 + 16J^2}{r_s^2}\right). \tag{24}$$

Substituting the functions above in (21) the resulting equation reads

$$r^2\frac{d^2R}{dr^2} + r\frac{dR}{dr} + R\left\{\left[\frac{1}{\sigma_1^2}\left(\omega - \frac{4Jm}{r_s^2}\right)^2 - k^2 - \beta^2\right]r^2 - m^2\right\} = 0, \tag{25}$$

with Bessel functions as solutions.

For the ballpoint pen model the function $\mathcal{X}$ and the determinant of the metric g are

$$\mathcal{X} = \frac{\sin^2(\sqrt{\lambda}r)}{\sqrt{\lambda}} = -g. \tag{26}$$

Using (21) we obtain

$$\sin^2(x)\frac{d^2R}{dx^2} + \sin(x)\cos(x)\frac{dR}{dx} + R\left[\frac{(\omega^2 - k^2 - \beta^2)\sin^2(x)}{\lambda} - (m + 2\alpha\omega f)^2\right] = 0, \tag{27}$$

with the function f given by

$$f = (r - r_s)\cos(x) - \frac{\sin(x)}{\sqrt{\lambda}} + r_s, \tag{28}$$

where $x = \sqrt{\lambda}r$. Equation (27) cannot be solved exactly. However, an approximate solution has been obtained in the quasistatic limit, defined as $\sqrt{\lambda}r_s \ll 1$. When such a limit is used in (15), the angular momentum and the linear mass density become

$$J \sim 0 + \mathcal{O}(x^3), \qquad \mu \sim \frac{\lambda r_s^2}{8} + \mathcal{O}(x^3), \tag{29}$$

resulting in an exterior solution that behaves as a quasistatic solution. In this case Eq. (27) turns into Bessel equation,

$$x^2\frac{d^2R}{dx^2} + x\frac{dR}{dx} + R\left[\frac{(\omega^2 - k^2 - \beta^2)x^2}{\lambda} - m^2\right] = 0. \tag{30}$$

Another solution of (27) can be obtained in the limit of large values of m. The necessary condition to be satisfied in this limit depends on the interval of the radial coordinate. One can note that in the range $0 \le r \le r_s$ the function $f(r)$ is bounded. Therefore, the limit of large m is reached when

$$m \gg \max_{r\in[0,r_s]} |2\alpha\omega f(r)|, \tag{31}$$

and (27) becomes

$$\sin^2(x)\frac{d^2R}{dx^2} + \sin(x)\cos(x)\frac{dR}{dx} + R\left[\frac{(\omega^2 - k^2 - \beta^2)\sin^2(x)}{\lambda} - m^2\right] = 0. \quad (32)$$

This equation is solved by associated Legendre functions.

IV. BOUNDARY CONDITIONS, CAUSALITY, QUASINORMAL MODES

A. Boundary conditions

In the static cosmic cylinder backgrounds, the space-time is divided in two different regions. Therefore, we need to specify junction and boundary asymptotic conditions. Namely, the scalar field in the interior region Ψ^{in} must be regular at the origin, the field and its derivative must be continuous on the border r_s of the cosmic cylinder, and only outgoing waves can escape to infinity. Hence, these boundary conditions can be summarized as

$$|\Psi^{\text{in}}| < \infty \quad \text{when } r \to 0, \quad (33)$$

$$\Psi^{\text{in}} = \Psi^{\text{out}}, \qquad \frac{\partial\Psi^{\text{in}}}{\partial x^\mu} = \frac{\partial\Psi^{\text{out}}}{\partial x^\mu} \quad \text{when } r = r_s, \quad (34)$$

$$\Psi^{\text{out}} \sim \frac{e^{-i\omega(t-r)}}{\sqrt{r}} \quad \text{when } r \to \infty, \quad (35)$$

where ω is a complex frequency of oscillation the scalar field. When the space-time does not have a regular interior region, as the static cosmic string, only (33) and (35) are used as boundary conditions. In the case of rotating space-times we need additional conditions to make the quasinormal mode problem well posed. The difficulty is related to the fact that the space-times under consideration are not globally hyperbolic. Although this is not an insuperable obstacle, further considerations must be made [11,17–19].

Specifically, there is a region $r < r_{\text{ctc}}$ where the temporal coordinate is not globally well defined because the vector fields $\partial/\partial t$ and $\partial/\partial\phi$ are timelike. A compact temporal coordinate ϕ leads to closed timelike curves. To deal with this problem we follow the approach developed by Novikov, Thorne, Friedman and others, imposing a ''self-consistency principle''[11], which roughly states that all events on CTCs influence each other around closed timelike lines in a self-adjusted way. One implementation of the self-consistency principle in the dynamical systems discussed in this article is done imposing that the propagation of scalar field is periodic in the space-time regions that are identified. Labeling these regions by Γ_i and Γ_f, we impose $\Psi(\Gamma_i) = \Psi(\Gamma_f)$. In the case of rotating cosmic cylinder space-times, this condition is satisfied in the causal region. What we need to do is to extend this condition to the noncausal region. We have

$$\Psi(t, 0, r, z) = \Psi(t, 2\pi, r, z) \Rightarrow \Phi(0) = \Phi(2\pi). \quad (36)$$

With this supplementary condition, the propagation of scalar fields becomes tractable.

B. Causality

In this section an analysis concerning causality is presented. One relevant characteristic of the considered class of space-times discussed in this work is the possibility of closed timelike curves. For metrics with the form presented in Eq. (1), they occur when $\tilde{L}(r)$ has a simple positive real zero r_{ctc}. In our space-times, the noncausal region are infinitely long hollow cylinders.

The $g_{\phi\phi}$ components of the static cosmic string and cylinder are always positive-definite if $\mu < 1/4$. Thus, the static cases can be declared causally well behaved. The rotating cases need to be analyzed one by one.

The rotating cosmic string admits a noncausal region with arbitrary size depending on the constants μ and J. In Fig. 1 one can see how these constants change the size of the noncausal region. There is no restriction for values of J but the linear mass density must be bounded.

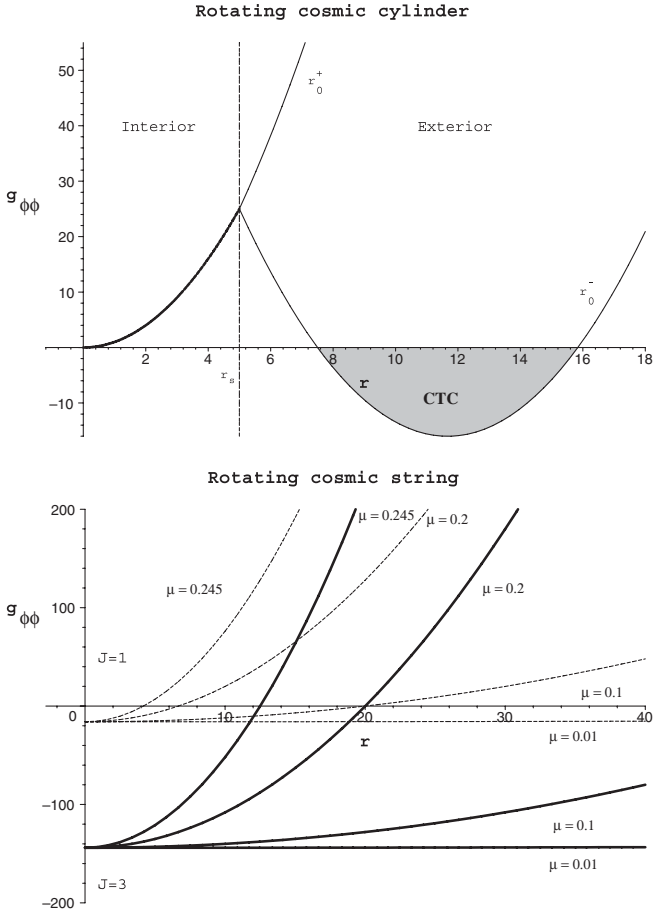

FIG. 1. The interior and exterior component $g_{\phi\phi}$ of the flower pot model for r_0^+ and r_0^- in (37) with $r_s = 5$ (top). The component $g_{\phi\phi}$ for the rotating cosmic string with different values of J and μ (bottom).

The other two cases of rotating cosmic cylinders are more complex than the rotating cosmic string. For simplicity, we choose to preserve the interior region, which contains matter, against CTCs, reducing the range of the parameters. The exterior of the rotating cosmic cylinder may have CTCs. In the case of the flower pot model the interior $g_{\phi\phi}$ component is always positive-definite, and therefore there is no CTC. In the exterior, the condition to have CTCs depends essentially on r_0 being given by

$$r_{\rm ctc} < \frac{\sqrt{16J^2}}{(1-4\mu)} - r_0, \quad \text{with}$$
$$r_0 = r_0^{\pm} = \pm\sqrt{\frac{r_s^2 + 16J^2}{(1-4\mu)^2}} - r_s. \tag{37}$$

If $|r_0|$ is large enough $r_{\rm ctc} < r_s$, resulting in the absence of a noncausal region. In Fig. 2 we show the position of the noncausal limit surface $r_{\rm ctc}$ for the rotating cosmic cylinder with the flower pot model.

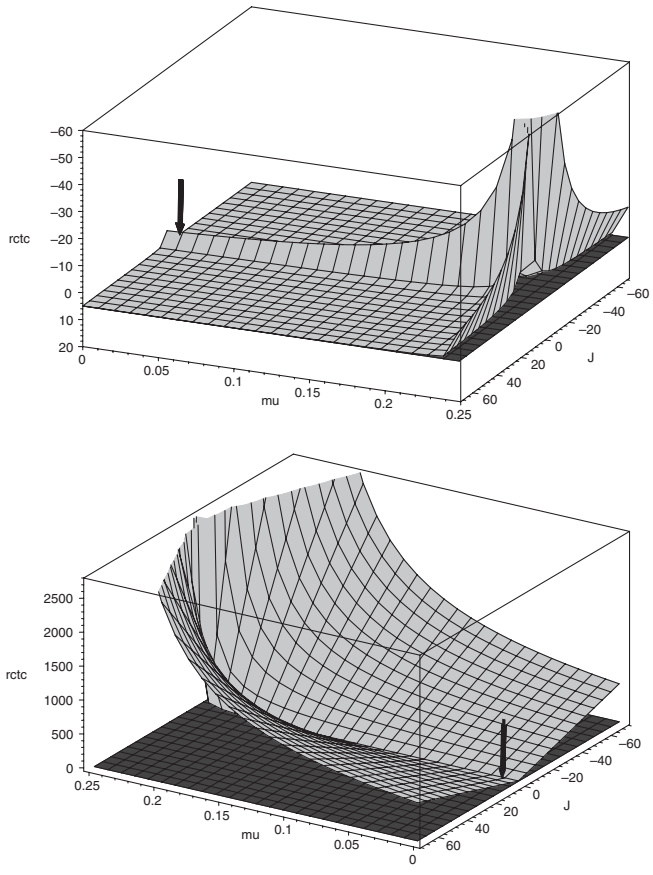

FIG. 2. Position of the noncausal limit surface $r_{\rm ctc}$ in the rotating cosmic cylinder with "flower pot model for r_0^+ (top) and r_0^- (bottom) in (37). The radius of the cosmic string is $r_s = 5$. The dark surface indicates the position of r_s, and the grey surface indicates the position of the noncausal limit surface $r_{\rm ctc}$. The black arrow shows the position of the noncausal limit surface for $\mu = 1.0 \times 10^{-2}$ and $J = 1$.

When the constant r_0^+ is chosen in (37), the noncausal limit surface always lies before r_s, as seen in Fig. 2 (top). In this case the exterior of the cosmic cylinder does not have CTCs. On the other hand, when the constant r_0^- is chosen the noncausal limit surface always lies after r_s allowing CTCs. It is shown in Fig. 2 (bottom). This conclusion is independent of the value of r_s. Therefore, in this case there is no restriction for the value of J. We still have $\mu < 1/4$. Figure 1 shows the causal behavior of the interior and exterior $g_{\phi\phi}$ components for the flower pot model.

For the ballpoint pen model, both the interior and exterior metrics allow the presence of CTCs. In this model a general analysis is quite difficult because of the number of free parameters. Each case must be analyzed independently, verifying whether the set of chosen constants satisfies given restrictions. The causal structure of this spacetime will depend on the adjustment of three constants r_s, λ and α. Analyzing the interior $g_{\phi\phi}$ component we can see that it can assume negative values. Recalling that we do not want CTCs in the interior solution, the set of constants must be chosen such that $g_{\phi\phi}$ is positive-definite. Again, the linear mass density must satisfy $\mu < 1/4$ and $\sqrt{\lambda} r_s < \pi/2$. The angular momentum is fixed by the choice of r_s, λ, and α.

As an example which captures the essence of the argument to be developed here, the set of constants $\lambda = 1.0 \times 10^{-3}$, $\alpha = 0.2$, and $r_s = 1$ keeps the interior $g_{\phi\phi} > 0$; i.e., it is causally well behaved. Now we need to analyze whether the set of chosen parameters allows the presence of CTCs in the exterior. For the exterior of the ballpoint pen model, the condition to have CTCs also depends on r_0, being given by

$$r_{\rm ctc} < \frac{\sqrt{16J^2}}{(1-4\mu)} - r_0, \quad \text{with}$$
$$r_0 = r_0^{\pm} = \pm\frac{\sqrt{1-(1-4\mu)^2}\, r_s}{(1-4\mu)\arccos(1-4\mu)} - r_s. \tag{38}$$

In Fig. 3 the position of the noncausal limit surface $r_{\rm ctc}$ for the rotating cosmic cylinder with the ballpoint pen model in the quasistatic limit is shown.

When the constant r_0^+ is chosen in (38), the position of the noncausal limit surface depends on the value of λ. For the particular case $\lambda = 10^{-3}$ and $\alpha = 0.2$, $r_{\rm ctc}$ is smaller than r_s, and in the exterior of this cosmic cylinder we do not find CTCs. If we choose $r_0 = r_0^-$ in (38) the position of the noncausal limit surface also depends on λ. But in this case $r_{\rm ctc}$ is bigger than r_s allowing CTCs. These considerations are general. Constraints on the values of λ and α result in restrictions for J and μ. Therefore, the angular momentum and linear mass density cannot assume arbitrary values in the ballpoint pen model.

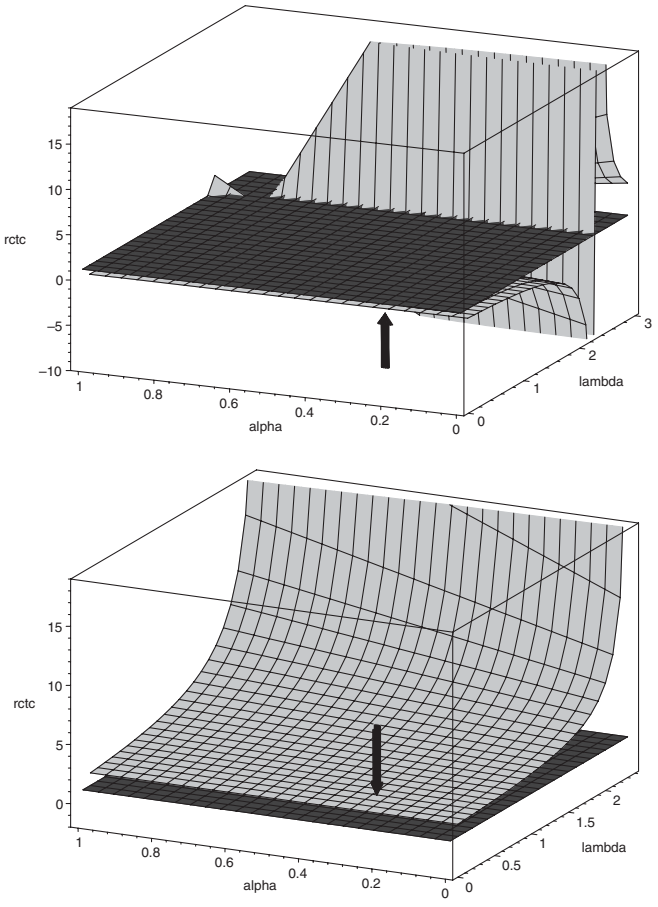

FIG. 3. Position of the noncausal limit surface $r_{\rm ctc}$ in the rotating cosmic cylinder with "ballpoint pen model for r_0^+ (top) and r_0^- (bottom) in (38). The radius of the rotating cosmic cylinder is $r_s = 1$. The dark surface indicates the position of r_s, and the grey surface indicates the position of the noncausal limit surface $r_{\rm ctc}$. The black arrow shows the position of the noncausal limit surface for $\lambda = 1.0 \times 10^{-3}$ and $\alpha = 0.2$.

C. Quasinormal modes

In this section we show the exact solutions for the evolution of the scalar field in the cosmic cylinder backgrounds. Quasinormal modes are numerically calculated.

1. Static cosmic cylinder

The boundary conditions (33) and (35) result in

$$R^{\rm in}(r) = \tilde{C}_1 P_n^m(\cos(r/\bar{r}_0)), \tag{39}$$

$$R^{\rm out}(r) = \begin{cases} C_1 H_\nu^1(pr) & \text{when } \omega_R > 0 \\ C_2 H_\nu^2(pr) & \text{when } \omega_R < 0, \end{cases} \tag{40}$$

where $n(n+1) = (\omega^2 - k^2 - \beta^2)\bar{r}_0^2$, $\nu^2 = m^2/(1-4\mu)^2$, and $p^2 = (\omega^2 - k^2 - \beta^2)$. The functions $R^{\rm in}$ and $R^{\rm out}$ are the radial part of the scalar field inside and outside of the cosmic cylinder. One can note that $R^{\rm out}$ depends on the sign of the real part of ω, due to the asymptotic behavior of Hankel functions. At the boundary, condition (34) implies

$$\frac{R'^{\rm in}(r_s)}{R^{\rm in}(r_s)} - \frac{R'^{\rm out}(r_b)}{R^{\rm out}(r_b)} = 0, \tag{41}$$

where $'$ denotes a derivative with respect to r. The parameters are related by

$$\begin{aligned} r_s &= \bar{r}_0 \theta_M, \qquad (1-4\mu) = \cos(\theta_M), \\ r_b &= \frac{\bar{r}_0 \sin(\theta_M)}{(1-4\mu)}, \qquad \rho = \frac{1}{8\pi \bar{r}_0^2}. \end{aligned} \tag{42}$$

If we choose ρ and r_s, the other constants are fixed and we need only calculating the zeros of (41) for given k, m, β to obtain the quasinormal frequencies ω. Some quasinormal modes for a static cosmic cylinder were numerically calculated. They are shown in Table I.

If we display the quasinormal modes in the $\omega_I \times \omega_R$ plane, we can see that the positive and negative ω_R of the quasinormal modes are distributed symmetrically with respect to the ω_I axis. This symmetry, which happens for any value of m, can be understood analytically as follows. For the nonrotating case, the external solutions, given in terms of the Hankel functions H_1 and H_2, transform into one another by changing the sign of the real part of ω. This, together with the invariance of the wave equation under complex conjugation, is in the basis of the symmetry $\omega \rightarrow -\omega^*$, as expressed in the solution. This argument breaks in the rotating case due to the correction proportional to $J\omega$, as discussed in the next section.

The finiteness of the obtained solutions is controlled by the imaginary part of the quasinormal frequencies ω_I. It is

TABLE I. Quasinormal modes for static cosmic cylinder with the parameters $r_s = 5.0$, $\rho = 1.0 \times 10^{-3}$, $\bar{r}_0 = 6.3$, $\mu = 0.1$, $r_b = 6.4$, $\beta = 0$, $k = 0$. Fundamental ($n = 1$) and high overtone modes ($n > 1$) for $m = 0$ (top). Fundamental mode ($n = 1$) for several values of m (bottom).

n	$\omega_R + i\omega_I$	
1	$-0.66 - i0.54$	$+0.66 - i0.54$
2	$-1.33 - i0.65$	$+1.33 - i0.65$
3	$-1.98 - i0.72$	$+1.98 - i0.72$
4	$-2.62 - i0.78$	$+2.62 - i0.78$
5	$-3.25 - i0.82$	$+3.25 - i0.82$
6	$-3.89 - i0.85$	$+3.89 - i0.85$
7	$-4.52 - i0.88$	$+4.52 - i0.88$
8	$-5.15 - i0.91$	$+5.15 - i0.91$

m	$\omega_R + i\omega_I$	
0	$-0.66 - i0.54$	$+0.66 - i0.54$
1	$-0.21 - i0.42$	$+0.21 - i0.42$
2	$-0.49 - i0.51$	$+0.49 - i0.51$
3	$-0.76 - i0.58$	$+0.76 - i0.58$
4	$-1.01 - i0.63$	$+1.01 - i0.63$
5	$-1.26 - i0.68$	$+1.26 - i0.68$
6	$-1.51 - i0.72$	$+1.51 - i0.72$
7	$-1.76 - i0.76$	$+1.76 - i0.76$

always negative, indicating stability of the static cosmic string against scalar perturbations. For $k \neq 0$ and $\beta \neq 0$ the position of modes is pushed away from the ω_R axis but the quasinormal spectrum qualitative behavior is the same.

2. Rotating cosmic cylinder

We now consider the rotating cosmic cylinder with the interior solution of the flower pot model. Applying the boundary conditions (33)–(36) to the scalar field, we have

$$\frac{R'^{\text{in}}(r_s)}{R^{\text{in}}(r_s)} - \frac{R'^{\text{out}}(r_s)}{R^{\text{out}}(r_s)} = 0. \tag{43}$$

The functions R^{in} and R^{out} are given by

$$R^{\text{in}}(r) = \tilde{C}_1 J_m(p_1(r)), \tag{44}$$

$$R^{\text{out}}(r) = \begin{cases} C_1 H^1_\nu(p(r+r_0)) & \text{when } \omega_R > 0 \\ C_2 H^2_\nu(p(r+r_0)) & \text{when } \omega_R < 0, \end{cases} \tag{45}$$

where $p_1^2 = \frac{1}{\sigma_1^2}(\omega - 4Jm/r_s^2)^2 - k^2 - \beta^2$, m is an integer, and $\nu^2 = (m + 4J\omega)^2/(1 - 4\mu)^2$. Once more the parameters associated to the space-time are related by

$$r_0 = r_0^{\pm} = \pm\sqrt{\frac{r_s^2 + 16J^2}{(1-4\mu)^2}} - r_s, \qquad \mu < \frac{1}{4}. \tag{46}$$

If we choose three constants, μ, J, and r_s, the constant r_0 is fixed and then we need only to calculate the zeros of Eq. (43) for specific values of k, m, β to obtain the quasinormal frequencies.

In Table II some numerically computed frequencies are shown for a rotating cosmic cylinder with the flower pot model. In contrast to the static case, here the distribution of ω_R is not symmetric with respect to the ω_I axis. The imaginary part ω_I can assume negative or positive values depending on the values of r_0^- in (46). The presence of modes with $\omega_I > 0$ indicates instabilities of the scalar field perturbation. On the other hand, if we choose the constant r_0^+ in (46), these unstable modes are absent. In this case, the space-time can be considered stable. The relation between $r_0^{\pm}$ and the stability issues will be discussed in Sec. V.

For the rotating cosmic cylinder with the ballpoint pen model, the quasinormal modes have been obtained in two different limits, namely, the quasistatic limit and large m limit. Again the same procedure described before can be used for both limits, imposing the same boundary conditions.

The boundary conditions (33)–(36) in the quasistatic limit give again Eq. (43). The functions R^{in} and R^{out} are given by

$$R^{\text{in}}(r) = \tilde{C}_1 J_m(p_1(\sqrt{\lambda}r)), \tag{47}$$

$$R^{\text{out}}(r) = \begin{cases} C_1 H^1_\nu(p(r+r_0)) & \text{when } \omega_R > 0 \\ C_2 H^2_\nu(p(r+r_0)) & \text{when } \omega_R < 0, \end{cases} \tag{48}$$

where now $p_1^2 = (\omega^2 - k^2 - \beta^2)/\lambda$. The parameters associated to the space-time are related by

TABLE II. Quasinormal modes for rotating cosmic string with flower pot model with the parameters $J = 1.0$, $\mu = 1.0 \times 10^{-2}$, $r_s = 5.0$, $\beta = 0$, $k = 0$, $r_0 = -12$ (top) and $r_0 = 1.7$ (bottom). Fundamental ($n = 1$) and high overtone modes ($n > 1$) for $m = 0$ (top). Fundamental mode ($n = 1$) for several values of m (bottom). The $*$'s indicate the unstable modes.

n	$\omega_R + i\omega_I$	
1	$0.064 + i0.041^*$	$-0.064 + i0.041^*$
2	$0.75 - i0.23$	$-0.21 + i0.044^*$
3	$1.57 - i0.32$	$-0.79 + i0.0082^*$
4	$2.39 - i0.36$	$-0.90 + i0.014^*$
5	$3.20 - i0.40$	$-1.46 + i0.031^*$
6	$4.01 - i0.43$	$-1.57 - i0.32$

m	$\omega_R + i\omega_I$	
0	$0.064 + i0.041^*$	$-0.064 + i0.041^*$
1	$0.026 - i0.055$	$-0.026 + i0.034^*$
2	$0.051 + i0.070^*$	$-0.56 + i0.026^*$
3	$0.15 - i0.22$	$-0.19 + i0.31^*$
4	$0.22 - i0.31$	$-0.37 + i0.042^*$
5	$0.29 - i0.39$	$-0.44 + i0.59^*$

n	$\omega_R + i\omega_I$	
1	$0.46 - i0.45$	$-0.46 - i0.45$
2	$1.23 - i0.57$	$-1.23 - i0.57$
3	$2.02 - i0.63$	$-2.02 - i0.63$
4	$2.83 - i0.67$	$-2.82 - i0.67$
5	$3.63 - i0.70$	$-3.63 - i0.70$
6	$4.43 - i0.73$	$-4.43 - i0.73$

m	$\omega_R + i\omega_I$	
0	$0.46 - i0.45$	$-0.46 - i0.45$
1	$0.94 - i0.39$	$-0.83 - i0.57$
2	$1.43 - i0.39$	$-0.12 - i0.15$
3	$1.90 - i0.40$	$-0.07 - i0.26$
4	$0.30 - i1.90$	$-0.17 - i0.30$
5	$0.83 - i2.09$	$-0.26 - i0.33$

$$r_0 = r_0^{\pm} = \pm\frac{\sqrt{1-(1-4\mu)^2}\,r_s}{(1-4\mu)\arccos(1-4\mu)} - r_s, \qquad \mu \sim \frac{\lambda r_s^2}{8} < \frac{1}{4}, \qquad J \sim 0. \tag{49}$$

Choosing λ and r_s, the other constants are fixed and we need only to compute the zeros of (43).

Quasinormal modes for the ballpoint pen model in the quasistatic limit were obtained numerically and are shown in the Table III. The imaginary part ω_I can assume negative or positive values depending on the values of $r_0^{\pm}$ in (49), as in the flower pot model. In the stable case, the first modes have higher ω_I than ω_R. This indicates that these modes are strongly damped. In the same way the presence of $\omega_I >$

0 would indicate instabilities of the scalar perturbation. However, if we choose r_0^+ in (49) these modes are absent.

Using the boundary conditions (33)–(36) in the large m limit, Eq. (43) is obtained with

$$R^{\text{in}}(r) = \tilde{C}_1 P_m^n(\cos(\sqrt{\lambda}r)), \tag{50}$$

$$R^{\text{out}}(r) = \begin{cases} C_1 H_\nu^1(p(r+r_0)) & \text{when } \omega_R > 0 \\ C_2 H_\nu^2(p(r+r_0)) & \text{when } \omega_R < 0, \end{cases} \tag{51}$$

where $n(n+1) = (\omega^2 - k^2 - \beta^2)/\lambda$. In Table IV some quasinormal modes for the rotating cosmic cylinder ballpoint pen model in large m limit are listed. The sign of the imaginary part ω_I depends again on the values of $r_0^\pm$. The presence of $\omega_I > 0$ indicates instabilities of the scalar perturbation. On the other hand, if we choose r_0^+ in (49) these modes are absent and we can declare the stability of the space-time under scalar perturbations. The precision of the approximation is higher in the first overtones. In this limit the field presents purely real modes of oscillation but they arise only when instabilities are also observed.

3. Static and rotating cosmic string

In the case of static and rotating string, the application of the boundary conditions (34) and (35) leads to Hankel functions. However when the regularity condition at the origin is imposed, both Hankel functions diverge. Hence

TABLE III. Quasinormal modes for rotating cosmic cylinder with ballpoint pen model in the quasistatic limit, with the parameters $J = 2.0 \times 10^{-5}$, $\mu = 1.0 \times 10^{-4}$, $r_s = 1.0$, $\beta = 0$, $k = 0$, $\alpha = 0.2$, $\lambda = 1.0 \times 10^{-3}$, $r_0 = -2.0$ (top) and $r_0 = 3.0 \times 10^{-4}$ (bottom). Fundamental ($n = 1$) and high overtone modes ($n > 1$) for $m = 0$ (top). Fundamental mode ($n = 1$) for several values of m (bottom). The $*$'s indicate the unstable modes.

n	$\omega_R + i\omega_I$	
1	$0.30 + i0.41^*$	$-0.30 + i0.41^*$
2	$2.96 - i0.94$	$-2.96 - i0.94$
3	$6.16 - i1.28$	$-3.83 + i0.18^*$
4	$9.33 - i1.47$	$-5.52 + i0.17^*$
5	$12.5 - i1.62$	$-6.16 - i1.28$
6	$15.6 - i1.73$	$-7.01 + i0.17^*$

m	$\omega_R + i\omega_I$	
0	$0.30 + i0.41^*$	$-0.30 + i0.41^*$
1	$1.84 + i0.25^*$	$-1.84 + i0.25^*$
2	$0.34 + i0.47^*$	$-3.06 + i0.27^*$
3	$1.10 + i0.70^*$	$-1.11 + i0.70^*$
4	$1.92 + i0.86^*$	$-1.92 + i0.86^*$
5	$2.76 + i0.99^*$	$-2.76 + i0.98^*$

n	$\omega_R + i\omega_I$	
1	$2.61 - i5.54$	$-2.61 - i5.54$
2	$5.94 - i5.72$	$-5.94 - i5.72$
3	$9.17 - i5.87$	$-9.17 - i5.87$
4	$12.4 - i6.00$	$-12.4 - i6.00$
5	$15.5 - i6.10$	$-15.5 - i6.10$
6	$18.7 - i6.18$	$-18.7 - i6.18$

m	$\omega_R + i\omega_I$	
0	$2.61 - i5.54$	$-2.61 - i5.54$
1	$1.07 - i5.47$	$-0.66 - i5.46$
2	$2.74 - i5.54$	$-2.21 - i5.60$
3	$1.00 - i5.86$	$-0.53 - i5.90$
4	$2.37 - i6.15$	$-1.94 - i6.27$
5	$0.85 - i6.77$	$-0.49 - i6.81$

TABLE IV. Quasinormal modes for rotating cosmic cylinder with ballpoint pen model in the large m limit with the parameters $J = 0.1$, $\mu = 1.0 \times 10^{-2}$, $r_s = 10$, $\beta = 0$, $k = 0$, $\alpha = 1.0$, $\lambda = 1.0 \times 10^{-3}$, $r_0 = -20$ (top) and $r_0 = 0.4$ (bottom). Fundamental ($n = 1$) and high overtone modes ($n > 1$) for $m = 70$ (top). Fundamental mode ($n = 1$) for several values of m (bottom). The $*$'s indicate the unstable modes and $\dagger$'s indicate the purely real modes.

n	$\omega_R + i\omega_I$	
1	$2.20^\dagger$	$-2.20^\dagger$
2	$2.47 + i3.99^*$	$-2.31 + i4.30^*$
3	$2.80 + i3.86^*$	$-2.84 + i4.08^*$
4	$2.96 + i3.78^*$	$-3.02 + i3.99^*$
5	$3.12 + i3.70^*$	$-3.20 + i3.90^*$
6	$3.29 + i3.61^*$	$-3.38 + i3.80^*$

m	$\omega_R + i\omega_I$	
60	$1.88^\dagger$	$-1.88^\dagger$
62	$1.94^\dagger$	$-1.94^\dagger$
65	$2.04^\dagger$	$-2.04^\dagger$
67	$2.10^\dagger$	$-2.10^\dagger$
70	$2.20^\dagger$	$-2.20^\dagger$
72	$2.26^\dagger$	$-2.26^\dagger$

n	$\omega_R + i\omega_I$	
1	$0.033 - i5.00$	$-0.15 - i4.70$
2	$0.21 - i5.00$	$-0.32 - i4.70$
3	$0.39 - i4.99$	$-0.48 - i4.69$
4	$0.57 - i4.98$	$-0.64 - i4.67$
5	$0.75 - i4.96$	$-0.81 - i4.66$
6	$0.93 - i4.94$	$-0.97 - i4.63$

m	$\omega_R + i\omega_I$	
60	$0.18 - i4.30$	$-0.10 - i4.05$
62	$0.19 - i4.44$	$-0.11 - i4.18$
65	$0.11 - i4.65$	$-0.045 - i4.38$
67	$0.11 - i4.79$	$-0.057 - i4.51$
70	$0.033 - i5.00$	$-0.16 - i4.71$
72	$0.039 - i5.14$	$-0.17 - i4.84$

these space-times do not display quasinormal modes of oscillation.

V. FINAL REMARKS

The results in this paper concern the stability of cosmic cylinder space-times and its relation to closed timelike curves. The data obtained in previous sections show that, when the parameters are chosen in a such way that the scalar quasinormal modes always have $\omega_I < 0$, then an inspection of the causal behavior reveals the absence of CTCs. On the other hand, if the parameters are chosen to guarantee the presence of CTCs in the space-time, then the scalar quasinormal modes will present unstable modes $\omega_I > 0$.

For the static cases and for the rotating cosmic strings and cylinders, it is observed that the solutions can be divided in two groups: the ''group S'', where r_0^+ is chosen in Eqs. (38), (46), and (49), and the ''group I'', where r_0^- is chosen. Thus the constant $r_0^\pm$ controls the appearance of CTCs in these cosmic cylinder space-times. The results can be stated schematically as

Scalar stability	Existence of CTCs
$\omega_I < 0$	$g_{\phi\phi} < 0$
$\Downarrow$	$\Downarrow$
group S:	group I:
r_0^+ in Eqs. (38) , (46) , (49)	r_0^- in Eqs. (38) , (46) , (49)
$\Downarrow$	$\Downarrow$
Absence of CTCs	Scalar instability
$g_{\phi\phi} > 0$	$\omega_I > 0$

Summarizing our results we conclude that cosmic cylinder space-times that present closed timelike curves are unstable against scalar perturbations. Since the scalar field propagation gives us strong signals of instabilities in the considered space-times when the CTCs are present, our results for the scalar perturbation lead us to conjecture that the presence of closed timelike curves is one source of *space-time* instabilities.

Our conjecture has some support in different scenarios, such as the Schwarzschild-Göedel background [20]. Such space-time is stable in the quasistatic limit (small angular momentum), as shown in [21]. And in this limit it is also possible to see that this geometry does not have closed timelike curves. A very interesting check would be a stability analysis in the large angular momentum limit of the Schwarzschild-Göedel solution, where closed timelike curves are present.

The better understanding of the relation between closed timelike curves and instabilities, or at least its extension to more general setups, could open a new window in the investigation of causality.

ACKNOWLEDGMENTS

The authors would like to thank FAPESP (Brazil) and CNPq (Brazil) for the financial support.

[1] J. Carot, J. Senovilla, and R. Vera, Classical Quantum Gravity **16**, 3025 (1999).
[2] Mikael Fjallborg, Classical Quantum Gravity **24**, 2253 (2007).
[3] Y. B. Zeldovich, Mon. Not. R. Astron. Soc. **192**, 663 (1980).
[4] J. R. Gott, III, Astrophys. J. **288**, 422 (1985).
[5] R. H. Brandenberger, A. T. Sornborger, and M. Trodden, Phys. Rev. D **48**, 940 (1993).
[6] A. Vilenkin and E. P. S. Shellard, *Cosmic Strings and Other Topological Defects* (Cambridge University Press, Cambridge, England, 1994).
[7] S. Deser and R. Jackiw, Comments Nucl. Part. Phys. **20**, 337 (1992).
[8] J. R. Gott, III, Phys. Rev. Lett. **66**, 1126 (1991).
[9] B. Jensen and H. H. Soleng, Phys. Rev. D **45**, 3528 (1992).
[10] M. S. Morris, K. S. Thorne, and U. Yurtsever, Phys. Rev. Lett. **61**, 1446 (1988).
[11] J. Friedman, M. S. Morris, I. D. Novikov, F. Echeverria, G. Klinkhammer, K. S. Thorne, and U. Yurtsever, Phys. Rev. D **42**, 1915 (1990).
[12] Pedro F. Gonzalez-Diaz, Phys. Rev. D **54**, 6122 (1996).
[13] E. Abdalla, B. Cuadros-Melgar, and A. G. Casali, Int. J. Theor. Phys. **43**, 801 (2004); Nucl. Phys. **B644**, 201 (2002).
[14] R. Gregory and R. Laflamme, Phys. Rev. D **51**, R305 (1995).
[15] W. A. Hiscock, Phys. Rev. D **31**, 3288 (1985).
[16] H. P. Nollert and B. G. Schmidt, Phys. Rev. D **45**, 2617 (1992).
[17] A. Ishibashi and A. Hosoya, Phys. Rev. D **60**, 104028 (1999).

[18] R. M. Wald, J. Math. Phys. (N.Y.) **21**, 2802 (1980); R. M. Wald and A. Ishibashi, Classical Quantum Gravity **20**, 3815 (2003).

[19] I. Ya. Arefeva, T. Ishiwatari, and I. V. Volovich, Theor. Math. Phys. **157**, 1646 (2008).

[20] Eric Gimon and Akikazu Hashimoto, Phys. Rev. Lett. **91**, 021601 (2003).

[21] R. A. Konoplya and Elcio Abdalla, Phys. Rev. D **71**, 084015 (2005).